Simultaneous Determination of Complex Refractive Index and Size Distribution of Airborne and Water-Suspended Particles from Light Scattering Measurements

By Masayuki Tanaka, Teruyuki Nakajima and Tamio Takamura*

Upper Atmosphere Research Laboratory, Tohoku University, Sendai 980, Japan
(Manuscript received 9 July 1982, in revised form 15 October 1982)

Abstract

To estimate the complex refractive indices and the size distributions of aerosols and hydrosols from light scattering measurements, we present a data processing technique using both inversion and library methods. Extensive numerical simulations have shown that the true values of complex refractive index and size distribution are retrieved fairly well when this method is applied to measurements of polarization components of scattered radiation parallel and perpendicular to the scattering plane.

1. Introduction

Inversion techniques to solve the Fredholm integral equation of the first kind have been applied to estimate the size distribution of airborne particles from spectral attenuation measurements and from light scattering measurements. However, a *priori* knowledge of the refractive index of particles necessary for these techniques is occasionally unobtainable when the measurements are performed in an ordinary atmosphere. In this connection, Yamamoto and Tanaka (1969) applied the Phillips-Twomey method to spectral attenuation measurements, where they assumed the refractive index of particles to be 1.5 to calculate the coefficient matrix of the basic linear equations. Such an assumption, however, is not necessarily correct in all the atmospheric conditions. So, they examined the errors involved in estimated values of the size distribution due to an uncertainty in the refractive index, and found that the error increases as the exponent of the power law of size distribution increases. Grassl (1971) and Badayev *et al.* (1975) also analyzed attenuation data by the iteration method and the statistical regularization method, respectively, and they pointed out that an adequate knowledge of the refractive index is necessary for successful solutions.

The relation between the intensity of singly scattered light and the size distribution of particles has the same form of the integral equation as in the attenuation measurement. Shifrin and Gashko (1974) examined the size distribution inverted by the statistical regularization method when the incorrect value of the refractive index is assumed, and found that, even if the random error involved in the measured phase function is as small as 0.1%, the obtained size distribution does not follow the true one. They showed that the incorrect assumption of the refractive index introduces the same effect as noticeable systematic errors in the measured phase function. Especially, adequate accuracy in the choice of the imaginary part of the refractive index is important for obtaining a successful solution.

On the other hand, several attempts to estimate the refractive index of airborne or water suspended particles by least-square fitting techniques have been made assuming some a priori forms of the size distribution, *i.e.* by the library method. Ward *et al.* (1973) analyzed polarization data for bistatic laser scattering to obtain best fit values of the complex refractive index and the exponent of a regularizing power law size distribution. Grams *et al.* (1974) obtained the value of imaginary part of the refractive index of soil-derived particles by minimizing the square deviation between the observed phase function and the theoretical one calculated for the log-normal size distribution giving the best

* Present affiliation: National Defence Academy, Yokosuka.

fit to the simultaneously observed size distribution. Gorchakov *et al.* (1976a) also applied essentially the same method to foggy haze data. Zanaveld *et al.* (1974) used the converging decent method to find the best fit combination of refractive indices and size distributions to account for the observed phase function of water-suspended particles. They found the suitable model was the two component system consisting of particles with refractive indices around 1.01–1.05 and 1.15, which obey the power law size distributions.

In this study, we present a method of simultaneous determination of the size distribution and the refractive index of airborne and water-suspended particles by combining the inversion technique of Phillips and Twomey with the library method mentioned above. Already, Gorchakov *et al.* (1976b) presented a similar method to ours to analyze the phase matrix data of foggy haze. We extend the library to include the imaginary part of the refractive index. The availability of the method is discussed as a preliminary model study of the data processing of real observation (see the paper following this study), taking account of both parallel and perpendicular polarization components of the scattered radiation. Retrievals of both size distribution and refractive index have also been attempted by Reagan *et al.* (1980) and Hansen (1980). Reagan *et al.* (1980) obtained the size distribution from spectral attenuation data, with which they selected most plausible values of the refractive index from the simultaneously observed bistatic lidar data. Hansen (1980) determined the complex refractive index and the exponent of the power law size distribution by a library method to interpret polar nephelometer data, similarly to Ward *et al.* (1973). He next improved the size distribution by a non-linear fitting technique using the refractive index obtained above. These authors have treated carefully the inference problems so that inference process of one variable, *i.e.* the refractive index or the size distribution, has minimum effect on inference process of another variable. It is worthwhile, however, to note that effective size range for inversion of data of various measurements or with various conditions differs from one another. Thus, it is very interesting to investigate efficiency of simultaneous fitting of more than one variable to interpret observed data.

2. Theory

We assume the polydispersion consisting of homogeneous dielectric spheres with the same refractive index $m=m_r-m_i i$. Validity of this assumption has become to be one of the most interesting problems in the atmospheric optics in the last decade (Powell *et al.* 1967; Holland and Gagne 1970; Chýlek *et al.* 1977; Heintzenberg and Welch 1982 and others). Although the general characteristics of difference between the scattering pattern of radomly oriented nonspherical particles and that of spheres are still open to discussion, it may come to an agreement that backward portion of the phase function of nonspherical particles depends less on the scattering angle than it does for spheres. Then, as pointed out by Grams *et al.* (1974), the value of imaginary part of the refractive index inferred from observation of the phase function must be regarded as the upper limit of the true value when the size distribution is known. In this context, Pinnick *et al.* (1976) tried to fit scattering patterns of nonspherical particles to those of spherical particles by introducing a fictitious absorption corresponding to imaginary part of the refractive index of 0.02–0.12.

Assuming scattering by spherical particles, observed polarization components of scattered radiation perpendicular and parallel to scattering plane (I_r, I_l) can be related to the corresponding incident radiation (I_{0r}, I_{0l}) as follows

$$\begin{bmatrix} I_r \\ I_l \end{bmatrix} = \frac{1}{r^2}\begin{bmatrix} \beta_1 & 0 \\ 0 & \beta_2 \end{bmatrix}\begin{bmatrix} I_{0r} \\ I_{0l} \end{bmatrix}. \qquad (1)$$

where r is the distance between the scattering volume and the observation point, and β_1 and β_2 are the phase functions given by

$$\beta_l(\Theta) = \frac{1}{k^2}\int_{a_{\min}}^{a_{\max}} |S_l(\Theta, ka, m)|^2 n(a)da \quad \text{for } l=1,2, \qquad (2)$$

where $k=2\pi/\lambda$: λ being the wavelength of light, a is the particle radius, $n(a)$ is the particle number spectrum, Θ is the scattering angle, and S_l is the scattering amplitude function calculated for particles with the complex refractive index m. Before approximating the above integral operation by an adequate finite sum, we conveniently take the volume spectrum instead of the number spectrum, *i.e.*

$$v(\ln a)d\ln a = \frac{4\pi}{3}a^3 n(a)da,$$

or

$$v(\ln a)=\frac{4\pi}{3}a^4 n(a)\,. \tag{3}$$

Substituting Eq. (3) into Eq. (2), we have

$$\beta_l(\Theta_i)=\int_{x_{\min}}^{x_{\max}} K_l(\Theta_i, x, m)v(x)dx \simeq \sum_{j=1}^{N} K_{lij}v_j \quad \text{for } l=1,2 \text{ and } i=1,2,\cdots,M\,, \tag{4}$$

where

$$x=\ln a\,, \tag{5}$$

$$K_{lij}=\int_{x_{j-1/2}}^{x_{j+1/2}} K_l(\Theta_i, x, m)dx\,, \tag{6}$$

$$K_l(\Theta, x, m)=\frac{3}{4\pi k^2 a^3}|S_l(\Theta, ka, m)|^2\,, \tag{7}$$

and v_j is a some representative value of $v(x)$ in the subinterval $(x_{j-1/2}, x_{j+1/2})$. Such a transformation is justified by reasons that (i) the kernel K_l is a rapidly oscillating function so that an averaging procedure is necessary to replace the integral by a finit sum, (ii) the kernel K_l averaged over a subinterval is a slowly varing function of x having the following asymptotic behaviors

$$K_l \propto \begin{cases} a^3 & \text{for } a\to 0 \\ a & \text{for } a\to\infty \text{ and } a\Theta\to 0 \\ 1/a & \text{for } a\to\infty \text{ and } a\Theta\to\infty \end{cases}\,, \tag{8}$$

and (iii) $v(x)$ is a slowly varing function of x because the typical number spectrum of airborne particles is the Junge's distribution of the form of $n(a)\propto a^{-4}$ (Toon and Pollack, 1976).

Dividing the Eq. (4) by the observed phase functions, we obtain a matrix equation

$$\boldsymbol{G}(m)\boldsymbol{V}=\mathbf{1}+\boldsymbol{\varepsilon}\,, \tag{9}$$

where

$$\boldsymbol{G}(m)=\begin{bmatrix}\boldsymbol{G}_1(m)\\ \boldsymbol{G}_2(m)\end{bmatrix} \text{ with } (\boldsymbol{G}_l(m))_{ij}=\frac{K_{lij}(m)}{\beta_l(\Theta_i)}\,, \tag{10}$$

and $(\mathbf{1})_i=1$. The error vector $\boldsymbol{\varepsilon}$ comes from several origins such as observational error, approximation by homogeneous spheres, finite sum approximation and so on. Inversion of the overdetermined system given by the Eq. (9) (with condition of $2M\geq N$), i.e. $\boldsymbol{V}'=(\boldsymbol{G}^*\boldsymbol{G})^{-1}\boldsymbol{G}^*\mathbf{1}$, where $\boldsymbol{G}^*$ is the transpose of $\boldsymbol{G}$, allows us the least square solution minimizing the relative error in the phase functions. The solution $\boldsymbol{V}'$ thus obtained, however, is generally an erroneous, highly fluctuating function of x because of inflation of the error vector $\boldsymbol{\varepsilon}$ in the process of matrix inversion (Twomey, 1963; Twomey and Howell, 1967; Dave, 1971). Several techniques to solve such a singular linear system have been presented: Phillips-Twomey method (Phillips, 1962; Twomey, 1963, 1965; Twomey and Howell, 1967), statistical regularization method (Turchin and Nozik, 1969; Shifrin *et al.*, 1972), iteration method (Grassl, 1971; Twitty, 1975), Backus-Gilbert method (Westwater and Cohen, 1973) and so on. We adopt the Phillips-Twomey method with the constraint condition to minimize the norm of the second derivative of the volume spectrum, *i.e.*

$$\int_{x_{\min}}^{x_{\max}}\left|\frac{d^2v(x)}{dx^2}\right|^2 dx\simeq \boldsymbol{V}\cdot\boldsymbol{H}\boldsymbol{V}\,, \tag{11}$$

where $\boldsymbol{H}$ is the finite difference representation of the fourth derivative operation d^4/dx^4. The least square solution for the Eq. (9) which allows the minimization condition of the Eq. (11) is

$$\boldsymbol{V}_c(m)=[\boldsymbol{G}^*(m)\boldsymbol{G}(m)+\gamma\boldsymbol{H}]^{-1}\boldsymbol{G}^*(m)\mathbf{1}\,. \tag{12}$$

This is essentially the same formula as for the statistical regularization method. Although approximate magnitude of the Lagrangean multiplier γ can be determined by several considerations (Turchin and Nozik, 1969; Dave, 1971), we simply select the optimum value of γ which minimizes the standard deviation σ given in Eq. (15) for each m, among the following prepared values

$$\gamma=\gamma_0\exp\left\{\frac{1}{N}\sum_{j=1}^{N}\ln(\boldsymbol{G}^*\boldsymbol{G})_{jj}\right\} \quad \text{with } \gamma_0=10^{-3}, 10^{-2}, \cdots, 10^2\,. \tag{13}$$

Further, we reassign the null value to negative values in the inverted size spectrum of the Eq. (12).

In the study of inversion problems, many authors have been interested in the degree of reconstruction of the size distribution, but have not compared in a systematic way the observed phase function with the reconstructed phase function

$$\mathbf{1}_c(m)=\boldsymbol{G}(m)\boldsymbol{V}_c(m)\,,$$

or,

$$\beta_{c,l}(\Theta_i, m)=\beta_l(\Theta_i)(\mathbf{1}_c(m))_i\,. \tag{14}$$

However, the degree of reconstruction can only be tested in terms of the observed quantities. Then, we investigate the standard deviation of relative error in $\beta_{c,l}$

$$\sigma(m)=\sqrt{|\mathbf{1}-\mathbf{1}_c(m)|^2/2M}\,. \tag{15}$$

It is natural to expect the deviation of the reconstructed phase function from the observed one will be large if an unrealistic value of the refractive index is assumed as pointed out by Gorchakov *et al.* (1976b) and Shifrin and Gashko (1974). The most plausible value of the refractive index of particles is, therefore, obtained by choosing the value $m=m_0$ at which the standard deviation σ in the Eq. (15) takes a minimum value. Correspondingly, the final estimation of the size distribution is given by $V_c(m_0)$.

3. Models and parameters

Seven polydispersions are selected to cover the range of variability of the size distribution of the tropospheric aerosols as shown in Fig. 1. In the figure, JUNGE-3, 4 and 5 show extensions of the power law size distribution first proposed by Junge (1955) in terms of the volume spectrum, *i.e.*,

$$v(x)=\begin{cases}\dfrac{4\pi A}{3}\exp(4x-lx_0) & \text{for } x\leq x_0\\ \dfrac{4\pi A}{3}\exp\{(4-l)x\} & \text{for } x>x_0\end{cases}, \tag{16}$$

where $x_0=\ln a_0$, $a_0=0.1\,\mu$m and $l=3$, 4 and 5. Toon and Pollack (1976) and Gorchakov and Yemilenko (1974) have shown that the JUNGE-4 is the good representative of the size distribution of aerosols in the lower troposphere. On the other hand, Deirmendjian (1969) has proposed that the size distributions of aerosols and clouds can be approximated by the modified gamma distribution, which is written in terms of the volume spectrum as

$$v(x)=\frac{4\pi A}{3}\exp\{(\alpha+4)x-\beta e^{\gamma x}\}\,. \tag{17}$$

We take his HAZE $L(\beta=15.1186,\ \alpha=2,\ \gamma=0.5)$, HAZE $M(\beta=8.944,\ \alpha=1,\ \gamma=0.5)$, and CLOUD $C1(\beta=1.5,\ \alpha=6,\ \gamma=1)$ models as the size distributions of continental aerosols, maritime aerosols and clouds, respectively.

The size distribution of aerosols sometimes reveals a multi-modal feature with superimposed background particle mode and soil-derived particle mode (Patterson, 1977). Volume spectrum named "BIMODAL" in Fig. 1 is the log normal approximation of a spectrum measured under conditions of slight visibility reduction

$$v(x)=\frac{4\pi A_1}{3}\exp\left\{4x-\frac{1}{2}\left(\frac{x-x_{m1}}{\ln S_2}\right)^2\right\}+\frac{4\pi A_2}{3}\exp\left\{4x-\frac{1}{2}\left(\frac{x-x_{m2}}{\ln S_2}\right)^2\right\}, \tag{18}$$

where $x_m=\ln a_m$ and involved parameters are $S_1=1.55$, $a_{m1}=0.0611$ and $A_1=1.77\times10^{-2}$ for the first mode, and $S_2=2.11$, $a_{m2}=0.232$ and $A_2=1.78\times10^{-5}$ for the second mode. The size range of particles is limited to $0.01\leq a\leq10\,\mu$m for all the spectra. Division points $\{x_{j-1/2}\}$ in the Eq. (4) are chosen with equidistant spacing as follows

$$x_{j-1/2}=0.64j-5.18 \quad \text{for } j=1,2,\cdots,12\,. \tag{19}$$

For such equidistant division points, the expression of the matrix $\boldsymbol{H}$ in the Eq. (11) is given by Yamamoto and Tanaka (1969). Angular division points $\{\Theta_i\}$ are chosen as 7(1) 10(2.5) 25(5) 170 degrees to meet the practical condition of our experiment (Takamura and Tanaka 1978).

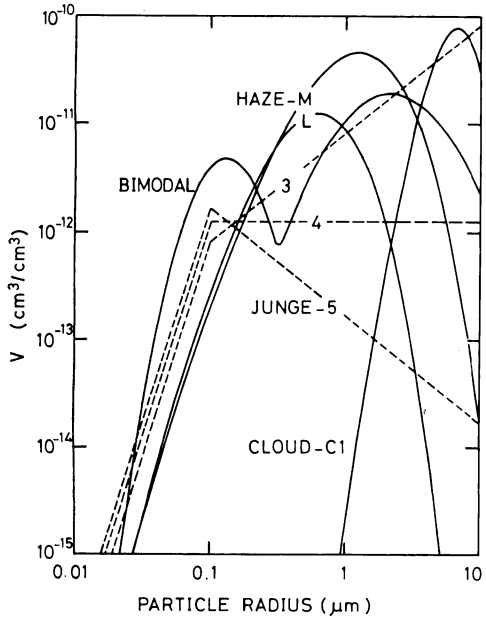

Fig. 1 Model volume spectra of airborne particles. For definition of each curve, see the text. Ordinate for the cloud is 10^3 times the values in the figure.

4. Analysis of the aerosol phase function

A typical example of our analysis is shown in Figs. 2, 3 and 4. Observed phase functions and corresponding values of the degree of linear polarization shown in Fig. 2 are estimated by adding Gaussian random errors $\varepsilon=\sqrt{\langle\boldsymbol{\varepsilon}\cdot\boldsymbol{\varepsilon}\rangle}$, where $\langle\ \rangle$ means averaged quantity, to the theoretical values calculated from Mie theory for the

JUNGE-3 aerosols with $m=1.55-0.01i$ at wavelength of $\lambda=0.5145\mu$m. By applying the Eq. (12) to the observed phase functions thus obtained (β_1 and β_2 in Fig. 2), we can infer the volume spectrum of aerosols corresponding to a specified value of the refractive index. As for the refractive index, we adopt the following set of values

$$m_r=1.45(0.05)1.65,$$

and

$$m_i=0.005, 0.01, 0.02, 0.03, 0.05 \text{ and } 0.08, \quad (20)$$

where m_r and m_i are the real and imaginary parts of the refractive index, respectively. Then, we apply the Eq. (14) to the spectra thus obtained and get a family of reconstructed phase functions. Two examples of the phase functions in this family are shown in Fig. 2 by solid and dashed lines. These examples represent the best and a rather poor fit corresponding to the volume spectra shown in Fig. 3 by circles and triangles, respectively.

We can now calculate the standard deviation of reconstructed phase functions from observed one, i.e. σ, by the Eq. (15). In Fig. 4 are shown numerical values of $\sigma-\sigma_{\min}$ for the case we concerned, where $\sigma_{\min}$ is the minimum value of σ. Since the value of $\sigma_{\min}$ is close to the value of ε, inherent random errors are subtructed from the total errors by such a procedure; the values of $\sigma-\sigma_{\min}$ roughly correspond to the systematic errors in reconstructed phase functions due to incorrect assumption of the refractive index. Drawing error contours on the table of the reconstruction errors in Fig. 4 we can find an acute minimum around the true value of the refractive index and, then, can infer the most plausible value of the refractive index as $m_0=1.55-0.01i$ which, in this case, is just identical with the true value.

In the course of model studies such as mentioned above, the following general properties

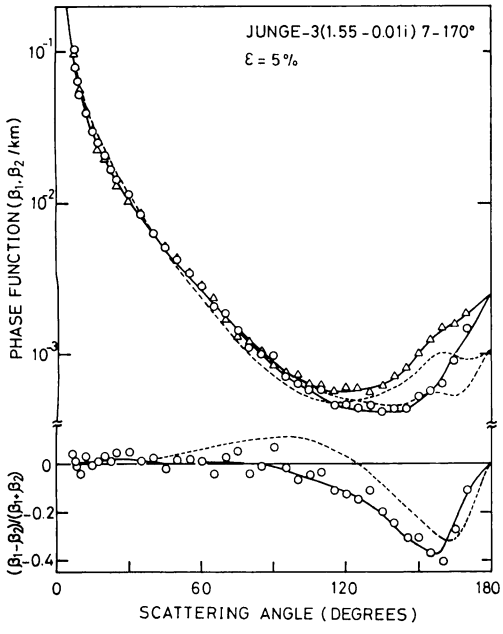

Fig. 2 Initially given and reconstructed phase functions: circles and triangles show initially given phase functions β_1 and β_2, respectively, calculated for the JUNGE-3 model with $m=1.55-0.01i$. Random observational error of 5% is assumed. Solid and broken lines show two examples of reconstructed phase functions, the best fit ($m_0=1.55-0.01i$, $\sigma-\varepsilon=0.002$, $\gamma_0=10^{-2}$) and a poor fit ($m_0=1.50-0.03i$, $\sigma-\varepsilon=0.12$, $\gamma_0=1$), respectively. Corresponding linear polarization $(\beta_1-\beta_2)/(\beta_1+\beta_2)$ is also shown in the lower part of the figure.

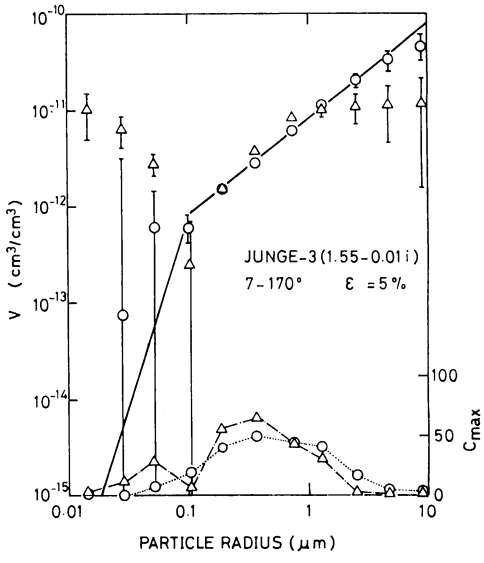

Fig. 3 Initially given and inverted volume spectra: solid line indicates initially given volume spectrum corresponding to the phase functions shown in Fig. 2, circles with error bars the best fit ($m_0=1.55-0.01i$, $\gamma_0=10^{-2}$) and triangles with error bars the poor fit ($m_0=1.50-0.03i$, $\gamma_0=1$). The maximum contribution, $C_{\max,j}$ of each size interval is shown in per cent in the lower part of the figure.

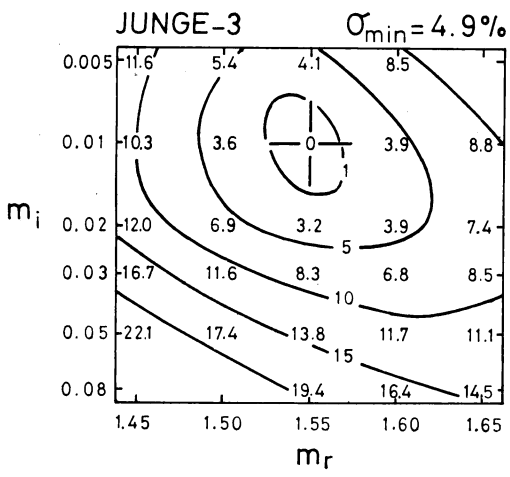

Fig. 4 Table of reconstruction errors $\sigma-\sigma_{\min}$ (in per cent) for initially given phase functions shown in Fig. 2. Abscissa and ordinate are the real and imaginary parts of the refractive index, respectively. Cross bars at $1.55-0.01i$ indicate the true value of the refractive index.

are observed for spherical particles: (i) the backward portion of the phase function is very sensitive to the trial values of the refractive index, (ii) the steepness of the forward portion of the phase function also contains useful information for determining the refractive index, (iii) the acute minimum of $\sigma-\sigma_{\min}$, if it were found, successfully shows the true value of the complex refractive index, (iv) extinction coefficients and single scattering albedos, as well as observed phase functions, are reproduced without significant errors from the assumed refractive index and the corresponding size distribution thus derived, (v) the relative root mean square deviations (*RMSD*) of the reconstructed volume spectrum (Turchin and Nozik, 1969) and the maximum contribution of a given spectral portion (say the j-th portion) to any portion of the phase functions defined respectively by Eqs. (21) and (22) provide good criterions for specifying reliability of our inversion

$$RMSD=\sqrt{\langle v_j^2\rangle}/\langle v_j\rangle=\varepsilon\sqrt{(\boldsymbol{G}^*\boldsymbol{G}+\gamma\boldsymbol{H})_{jj}^{-1}}\,, \tag{21}$$

$$C_{\max,j}=\max\{K_{lij}v_j/\beta_l(\Theta_i) \quad l=1,2;\ i=1,2,\cdots,M\}. \tag{22}$$

In Fig. 3 are shown the values of *RMSD* and $C_{\max,j}$ by error bars and curves drawn in the lower part of the figure, respectively. For the correct value of the refractive index (i.e. $m_c=1.55-0.01i$), error bars are short and $C_{\max,j}$ values are large in the region of good reconstruction, whereas either error bars are long or $C_{\max,j}$ values are insignificant in the region of poor reconstruction. Thus, the information extracted from our inversion technique depends on the *RMSD* and $C_{\max,j}$ values defined by the Eqs. (21) and (22). However these criterions are no longer applicable when the refractive index is incorrect, since the kernel matrix K_{lij} in the Eq. (4) depends on the size distribution in different way from the true one. Therefore, plausible values of the refractive index should be determined by minimizing of the reconstruction error $\sigma-\sigma_{\min}$, before determination of the final volume spectrum. Once we obtain the most plausible value of the refractive index, our scheme can then be used to invert the volume spectrum. Errors involved in the inverted volume spectrum are found to be insignificant in the size range from 0.1 to 3μm for aerosol models shown in Fig. 1 except for the CLOUD C1 model, as expected from the result of Dave (1971).

Fig. 5 shows similar error contours to Fig. 4 for the six other models shown in Fig. 1. The true value of the refractive index and the observational error are assumed to be $m=1.55-0.01i$ and 5%, respectively. Observational scattering angles, $\Theta_i\in[7, 170]$, are given in Section 3. From Figs. 4 and 5, we can see that the validity of determination of the refractive index depends more or less on the form of the volume spectrum. As the modal radius of the volume spectrum increases, the reconstruction error becomes more sensitive to the imaginary part of the refractive index, whereas the sensitivity to the real part does not change seriously. Also, it is of interest to note the general tendency that the basin of the error contour tends to extend from the upper left to the lower right portions of the map. This property of error contours can be understood more clearly when we investigate the dependence of the phase functions in particle sizes and refractive indices. In Fig. 6 are shown the relative differences of the steepness of the phase functions calculated with various values of the refractive index from that calculated for a standard value of $m_0=1.55-0.01i$, *i.e.*

$$\sigma_l(\Theta_1,\Theta_2,m)=\Delta\beta_l(\Theta_1,\Theta_2,m)/\Delta\beta_l(\Theta_1,\Theta_2,m_0)-1\,, \tag{23}$$

where,

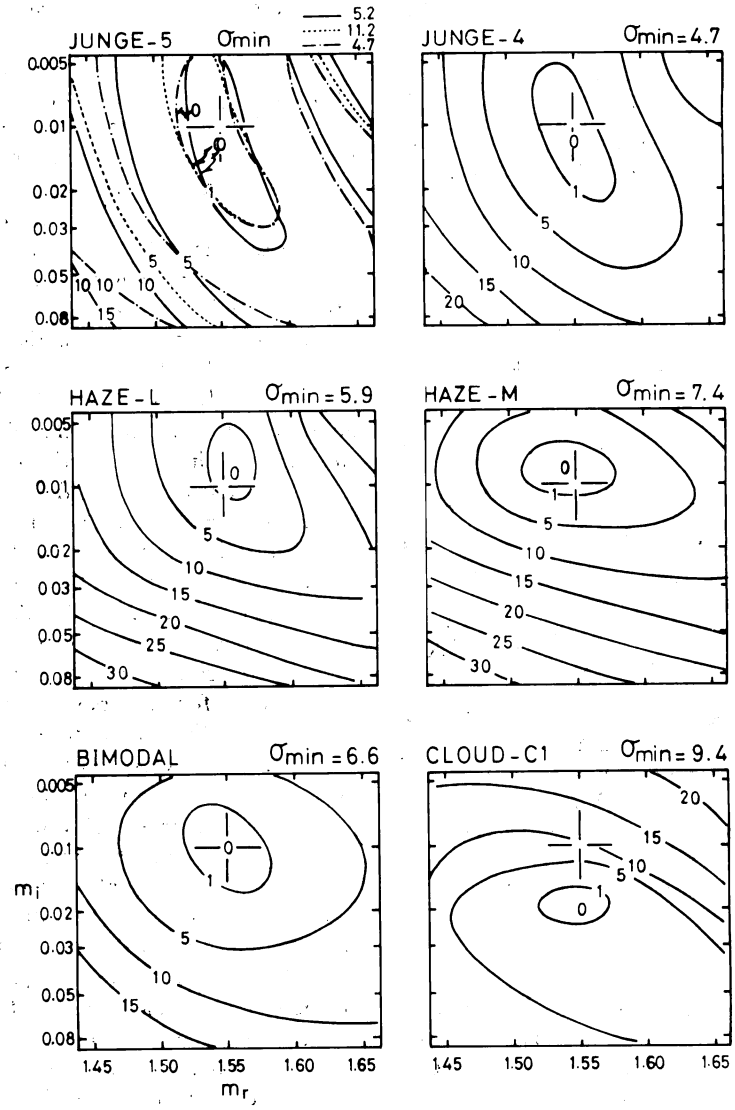

Fig. 5 As in Fig. 4 but for different aerosol models. Solid lines are for analyses of the phase functions with the observational error of 5% and the scattering angles of 7 (1) 10 (2.5) 25 (5) 170 degrees. Dotted and dashed-dotted lines in the figure for the JUNGE-5 model show the results for the observational error of 11% and for the entire scattering angle of [0, 180].

$$\Delta\beta_l(\Theta_1, \Theta_2, m) = \ln\{\beta_l(\Theta_1, m)/\beta_l(\Theta_2, m)\}. \quad (24)$$

For simplicity, we present only the result for the vertical polarization component ($l=1$). Three angular ranges of (25, 45), (45, 90) and (180, $\Theta_{\min}$), where $\Theta_{\min}$ is the scattering angle at which $\beta_l(\Theta)$ takes the minimum value, are investigated. Deirmendjian's HAZE *M* and *H* models are adopted as representative size distributions containing larger and smaller particles, respectively. The HAZE *H* model is calculated by the Eq. (17) with parameters $\beta=20$, $\alpha=2$ and $\gamma=1$ and, although not shown in Fig. 1, has the maximum around $a=0.3\mu$m. On the other hand, the HAZE *M* model has the maximum around $a=1.5\mu$m. The contour of $\sigma_1(\Theta_1, \Theta_2, m)$ for the HAZE *H* model depend less on the imaginary part of the refractive index than those for the HAZE *M*

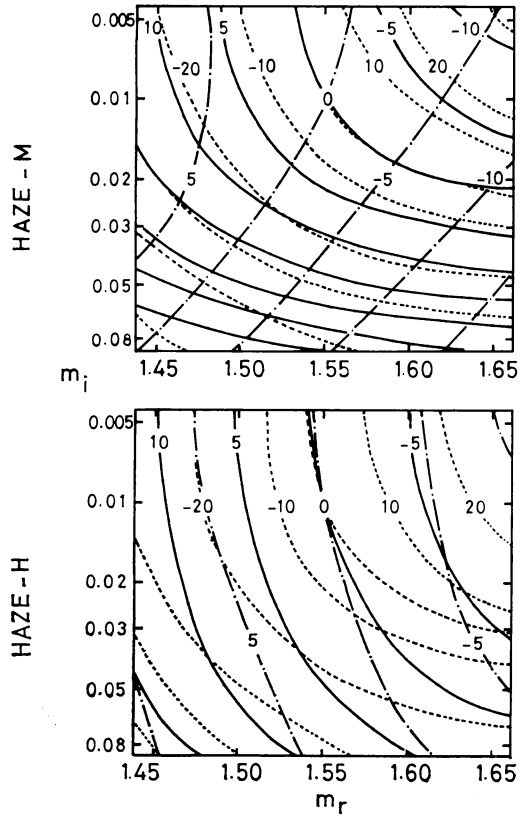

Fig. 6 Relative differences of the steepness of β_1 from that for $m_0=1.55-0.01i$ at wavelength of 0.45 μm. Solid, dashed-dotted and dotted lines indicate $\sigma_1(25, 45)$, $\sigma_1(45, 90)$ and $\sigma_1(180, \Theta_{\min})$.

model. To have a crude image of the scattering process by large ($ka\sim10$) and small ($ka\sim1$) particles, we have examined phase functions cauculated by the ray optics under the same condition as in Fig. 6, even though the ray optics is not a good approximation for Mie's solution unless the size parameter ka is larger than a few hundreds (Liou and Hansen, 1971). According to the ray optics, internal radiation in a large particle is rapidly absorbed as the imaginary part of the refractive index increases due to their long optical path in the particle. Thus the shape of the phase function drastically changes for large particles ($ka\sim10$) as the imaginary part of the refractive index increases in the range of $m_i\lesssim0.1$. On the other hand, the change is slight for small particles as long as m_i is not so large. Also, the ray optics is useful to understand the skewed pattern of the contour maps observed in Figs. 4 and 5. Since the intensity of the reflected ray is a slowly varying function of the scattering angle, the backward portion of the phase function becomes more flat as refracted rays decrease with increase (or decrease) of imaginary (or real) part of the refractive index. Thus, the backward portion of the phase function for particles with small values of both imaginary and real parts of the refractive index resembles that for particles with large values of both imaginary and real parts of the refractive index, as shown by dotted lines in Fig. 6. On the other hand, the forward portion of the phase function, say the phase function at scattering angles from 25 to 45 degrees, becomes more steeper either when the diffracted ray prevails with an increase of the imaginary part or when the anisotropy of the refracted ray increases with a decrease of the real part of the refractive index. Thus, the pattern of $\sigma_1(25, 45)$ on the refractive index plane is similar to that of $\sigma_1(180, \Theta_{\min})$, though directions of the gradient are opposite to each other. As the result, it is observed from Fig. 6 that a phase function with a steep forward portion is likely to have a flat tail in the backward portion. Therefore, if we use only the forward portion or the backward portion of the phase function, it is difficult to obtain a unique set of values of the real and imaginary parts of the refractive index. Fortunately, an intermediate angular region of the phase function depends in different way on each part of the complex refractive index as shown by dashed-dotted lines of $\sigma_1(45, 90)$ in Fig. 6. At these intermediate angles, the reflected ray prevails with the absorption, so that the phase function becomes rather flat as the imaginary part of the refractive index increases. Since this portion of the phase function also becomes flat with an increase of the real part of the refractive index, contours of $\sigma_1(45, 90)$ distribute from the upper left to the lower right of the map. In this way, the entire angular region of the phase function is required for a reliable estimate of the refractive index. Detailed investigation shows that $\sigma_1(25, 45)$ and $\sigma_1(180, \Theta_{\min})$ depend more sensitively on the refractive index than $\sigma_1(45, 90)$ does, so that the skewed pattern of error contours as shown in Figs. 4 and 5 will be found in general for an inversion utilizing phase functions alone. This implies that it is more or less difficult to distinguish the true value of the refractive index from an index of which real and imaginary parts are simultaneously overstimated

or underestimated.

Returning to Fig. 5, we examine the error contours in detail. Comparing the location of the minimum of the reconstruction error with the true value, it is seen that the errors in estimating the real and imaginary parts, are, respectively, less than 0.025 in absolute value and 1.2 in factor except for the case of the CLOUD C1 model. Fig. 5 also shows the results of two other experiments for the JUNGE-5 model; one is for the data containing random error of $\varepsilon = 0.1$, and the other is for the data sampled from the entire angular region $\Theta_i \in [0, 180]$ by adding new five angles of 0, 2, 4, 5.5 and 180 degrees. Since the basic patterns of the error contours hardly change with such modifications, it is expected that the refractive index can be determined with an accuracy comparable to this study for other experimental conditions.

Finally, we examine the case for which data are incomplete comparing with standard observation. Fig. 7 shows the error contours for analyses using forward portions of β_1 and β_2, backward portions of β_1 and β_2, the vertical component β_1 alone, the parallel component β_2 alone, and the averaged phase function $(\beta_1+\beta_2)/2$. The upper two maps are for the JUNGE-5 model and the lower two for the JUNGE-3 model. Comparing Fig. 7 with Figs. 4 and 5, we can see that each part of the phase function contributes in different manner to the estimation of the real and imaginary parts of the refractive index, and lack of the data reduces the reliability of inversion, as already pointed out. For a polydispersion containing small particles, such as the JUNGE-5 model, the imaginary part of the re-

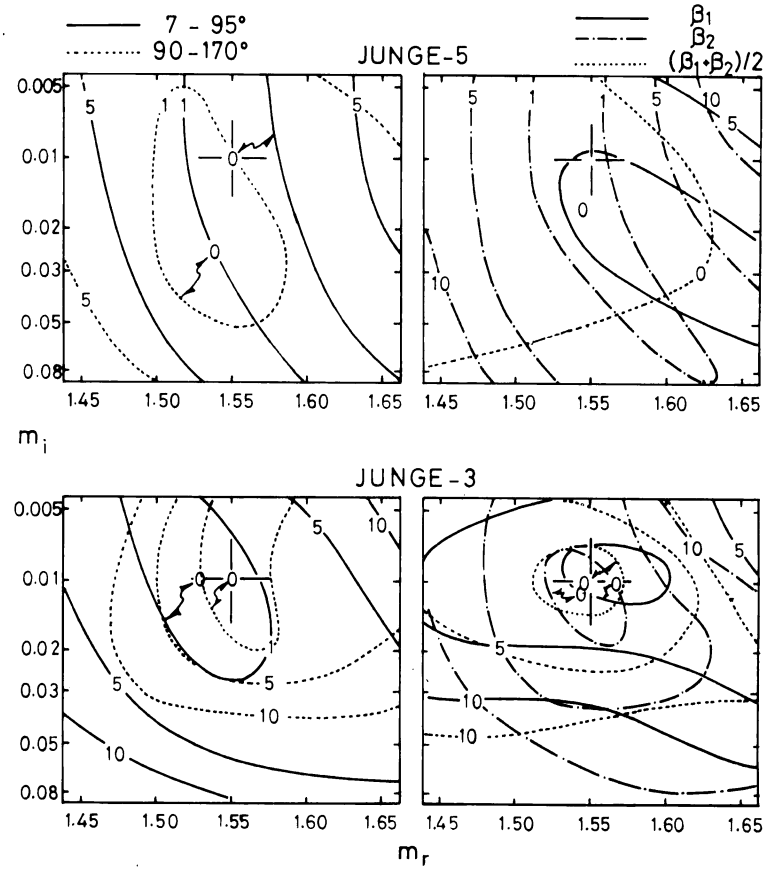

Fig. 7 As in Figs. 4 and 5, but for different experimental conditions; data for different parts of the standard phase functions with the observational error of 5%; forward and backward portions of β_1 and β_2 over the range of [0, 95] and [90, 180], respectively, vertical component β_1 alone, parallel component β_2 alone and the averaged phase function $(\beta_1+\beta_2)/2$.

fractive index cannot be estimated precisely in any case in the figure, and both the real and imaginary parts cannot be estimated either from β_1 alone or from the averaged phase function. On the other hand, for a polydispersion containing larger particles such as the JUNGE-3 model, the damage to the accuracy of the estimation is relatively slight and the interpolated minimum roughly indicates the true value.

Besides the phase functions, the extinction coefficient C_{ext} and the single scattering albedo $\omega_0 = C_{sca}/C_{ext}$ (C_{sca} being the scattering coefficient) can also be reconstructed from the inverted volume spectrum as shown in Table 1. It is important to note that; (i) an increase in the observational error from 5 to 10% has only a small effect on the accuracy of reconstruction, (ii) the single scattering albedo can be reconstructed with errors less than 5% and the extinction coefficient with errors less than 10%, except for the CLOUD C1 model. For the CLOUD C1 model, the scattering albedo can be estimated accurately despite the poor estimate of the extinction coefficient. This is due to the fact that the single scattering albedo approaches the asymptotic value of 0.5 for large absorbing particles.

The cause of breakdown in the estimation of the refractive index seen in the CLOUD C1 model can be explained when we examine the inverted volume spectrum. The volume spectrum of the CLOUD C1 model is nearly a delta function having a sharp maximum around the radius of 7μm, as shown in Fig. 1, so that only three columns of coefficient matrix K_{lij}, i.e. only three size intervals, can be utilized to construct the phase function. Thus, our size division given in the Eq. (19) is too coase for the CLOUD C1 model to adequately approximate the integral in the Eq. (2) by the finite sum, resulting in poor fit of the phase function and, consequently, an unreliable estimate of the refractive index. In this case, however, the large value of γ in the Eqs. (12) and (13) and the large value of σ compared with observational error ε can be regarded as symptoms for which the procedure should be modified with a suitable division of size intervals that are small enough for an adequate inversion. For the other six polydispersions in Fig. 1, it is unnecessary to reset the size intervals. This fact means that our size division in the Eq. (19) is not too coase to determine refractive indices and volume spectra of the lower tropospheric aerosols.

5. Analysis of hydrosol phase functions

Because the water has the refractive index of about 1.34 for the visible wavelength region, the refractive index of hydrosols is generally close to unity. According to our previous paper (Tanaka and Nakajima, 1977), expected values of the real part of the refractive index range from 1.05 to 1.20, while the values of imaginary part are highly uncertain. For numerical test of our method, we assume the following set of trial refractive indices

$$m_i = 1.05, 1.10, 1.20, 1.30, 1.35;$$

and

Table 1 Assumed and reconstructed extinction coefficients, C_{ext} and $C_{ext,c}$ in km^{-1} and corresponding single scattering albedos, ω_0 and $\omega_{0,c}$. Observed phase functions are for $m=1.55-0.01i$ and $\Theta=7$ (1) 10 (2.5) 25 (5) 170 degrees. Upper and lower figures in each row are for observational errors of 5 and 10%, respectively.

Model	C_{ext}	$C_{ext,c}$	%-error	ω_0	$\omega_{0,c}$	%-error
HAZE-M	0.156	0.154	−1.3	0.846	0.855	1.1
		0.170	9.0		0.814	−3.8
HAZE-L	0.0788	0.0808	2.5	0.905	0.895	−1.1
		0.0861	9.3		0.868	−4.1
CLOUD-C1	16.5	8.61	−47.8	0.584	0.606	3.8
		—	—		—	—
JUNGE-3	0.0706	0.0681	−3.5	0.795	0.801	0.8
		0.0659	−6.7		0.815	2.5
JUNGE-4	0.0218	0.0218	0.0	0.914	0.911	−0.3
		0.0226	3.7		0.904	−1.1
JUNGE-5	0.0125	0.0123	−1.6	0.939	0.939	0.0
		0.0124	−0.8		0.934	−0.5
BIMODAL	0.0709	0.0768	8.3	0.856	0.832	−2.8
		0.0767	8.2		0.828	−3.3

$$m_i = 0, 0.005, 0.01, 0.03, 0.05 . \quad (25)$$

The JUNGE-3 and -5 models are assumed for the size distribution because the Junge-type spectrum is typical again in the ocean. Fig. 8 shows the model phase functions with the refractive index of $1.05-0.01i$. Comparing with Fig. 2, β_2-component decreases drastically at the right scattering angle. The linear polarization changes very sensitively with variation of the real part of the refractive index as well as of the size distribution. This is very clearly supported by Fig. 9 which shows the reconstruction error for the simulated observation given in Fig. 8. Comparing Fig. 9 with Figs. 4 and 5, it is known that the sensitivity of estimation much increases for the real part of the refractive index, and the value of the real part of hydrosols' refractive index is determined very precisely if both of the phase functions β_1 and β_2 are available. If we have the averaged phase function $(\beta_1+\beta_2)/2$ alone, it is difficult to determine precisely the both parts of the complex refractive index as in the case for aerosols. Fig. 9 also shows that it is more or less difficult to determine the magnitude of the imaginary part of the refractive index, especially for size distributions abounding in small particles, such as the JUNGE-5 model.

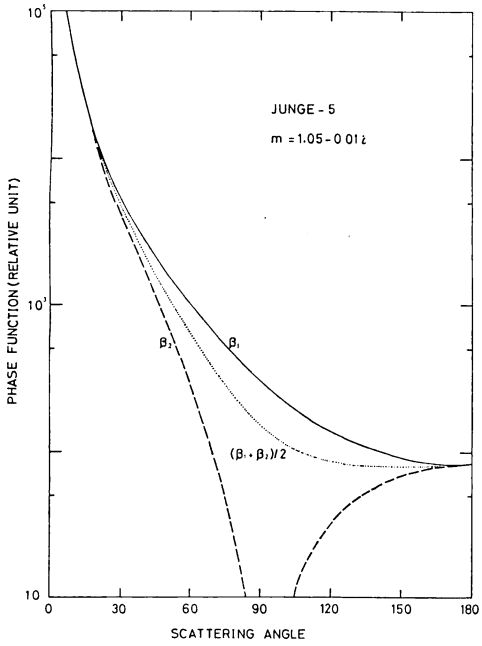

Fig. 8 Model phase functions for the JUNGE-5 hydrosols with $m=1.05-0.01i$ at wavelength of 0.5μm in vacuum.

Fig. 10 shows the inverted volume spectra: solid lines are the results for the full polarization set, and dashed lines for the averaged phase function. The results are shown for spectral ranges where the maximum contribution exceeds 10% because inverted size spectra out of this range do not follow the true values. In Fig. 10 are also shown examples of unsuccessful inversion by dotted lines. These poor estimations caused by inadequate selection of the trial refractive index are more serious for hydrosols than for aerosols. This can be understood if we recall the Rayleigh-Gans theory (van de Hulst, 1957). When the magnitude of the complex refractive index is very close to unity and the phase shift of the scattered electromagnetic wave is very small, the scattering efficiency factor for a dielectric sphere is given as follows

$$Q_{sca} = |m-1|^2 \varphi(ka) , \quad (26)$$

where φ is a function of only ka. If we choose the refractive index as $m=1.05-0.03i$ instead of the true value of $m_0=1.05-0.01i$, the Eq. (26) shows that the volume spectrum is underestimated by a factor about 0.77. On the other hand, if we choose $m=1.10-0.01i$ instead of $m_0=1.20-0.01i$, the volume spectrum is overestimated by a factor about 4. In this way, errors in the estimation of the complex refractive index introduces very serious errors in the retrieved volume spectrum in the case of hydrosols. Since hydrosols are always suspended in the medium as naked particles, the non-sphericity of particles is expected to be more noticeable for hydrosols than for aerosols. The results of the above analysis shows that this non-sphericity of hydrosols is a serious obstacle to successful inversion of the volume spectrum as well as to successful estimation of the refractive index of hydrosols.

6. Summary and problems

We have proposed a new method to estimate simultaneously the refractive index and the volume spectrum of aerosols or hydrosols. The applicability of the method is shown by numerical simulations for spherical particles. In summary, the following properties are observed: (i) the most plausible refractive index of a polydispersion is one which minimizes the reconstruction error σ; (ii) using the refractive index thus obtained, the volume spectrum can also be inferred for particles with radii from about 0.1 to 3μm; (iii) any portion of the inverted volume spectrum for which the maximum contribution

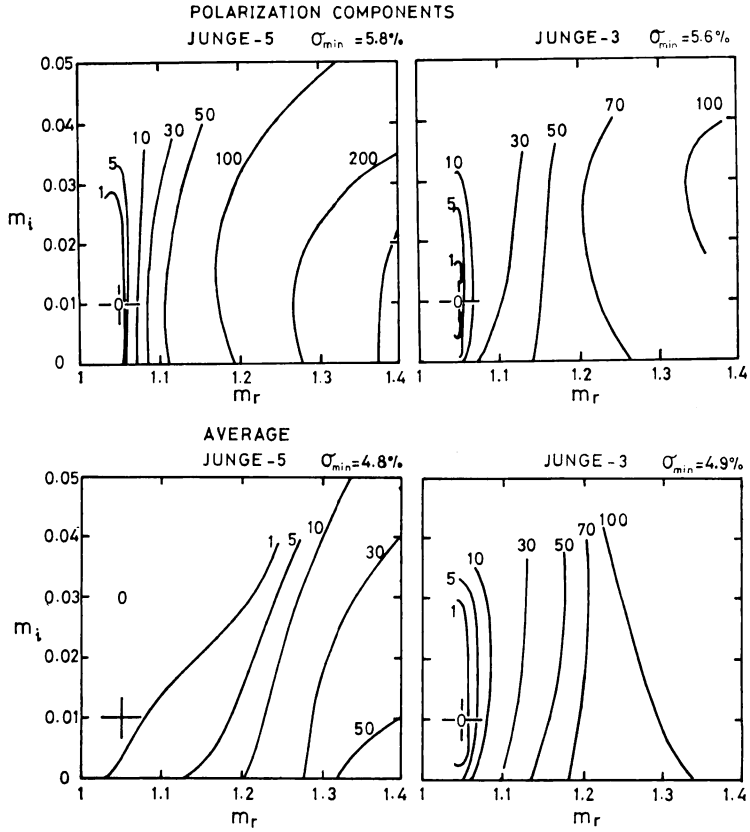

Fig. 9 Reconstruction errors $\sigma-\sigma_{\min}$ (in per cent) for hydrosol models with $m=1.05\text{-}0.01i$. Upper figures are for both components of the phase functions (β_1, β_2), and lower figures for average phase function $(\beta_1+\beta_2)/2$.

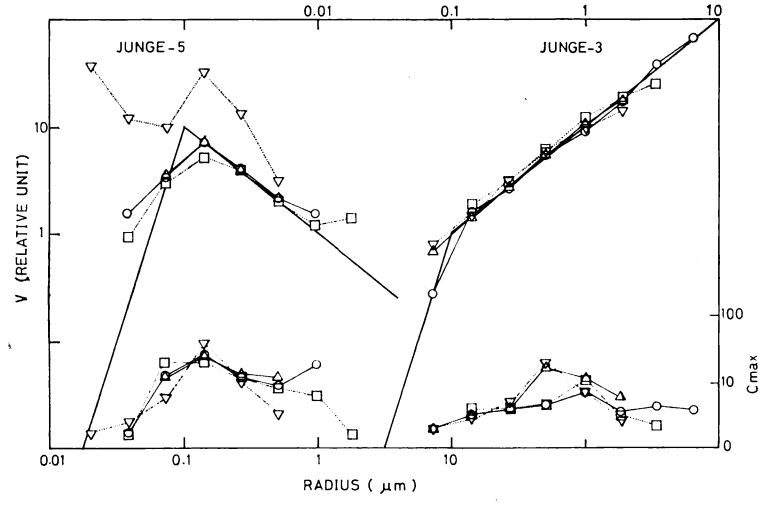

Fig. 10 Inverted volume spectra and their maximum contributions for the JUNGE-3 and -5 models. Initially given data are (β_1, β_2) for (○) and (△), and their average values $(\beta_1+\beta_2)/2$ for (□) and (▽). Assumed values of the refractive index are $m=1.05\text{-}0.01i$ for (○) and (□), and $m=1.20\text{-}0.01i$ for (△) and (▽). Most plausible values of the refractive index obtained are same as the true values excepting $m_0=1.05\text{-}0.03i$ for (□) and $m_0=1.10\text{-}0.03i$ for (▽).

in the Eq. (22) exceeds 10% is in close agreement with the true spectrum; (iv) reliability of estimation of the imaginary part of the refractive index increases when the polydispersion contains larger particles; (v) for a reliable analysis, both β_1 and β_2 must be observed over a wide range of the scattering angles.

Although our method is useful for a polydispersion of spherical particles, non-sphericity of the real particles, if it exist, will affect the accuracy so as to overestimate the imaginary part of the refractive index and, correspondingly, to leads to either underestimation or overestimation of particle number densities at specific size ranges. For future problems, the effects of non-sphericity of particles, especially for hydrosols, must be investigated. It is also interesting to investigate the efficiency of our method when it is applied to other types of data, such as spectral attenuation measurements, or to combinations of different types of data.

Acknowledgements

This study was supported by Research Project, Grant in Aid for Scientific Research of the Ministry of Education, Science and Culture, Japan, 1979 and 1980, Project Number 446037.

References

Badayev, V. V., Yu. S. Georgiyevskiy and S. M. Pirogov, 1975: Aerosol extinction in the spectral range 0.25-2.2 μm. *Izv.,, Atmos. Ocean. Phys.*, **11**, 522-526.

Chýlek, P., G. W. Grams and R. G. Pinnick, 1977: Light scattering by nonspherical particles, *Radiation in the Atmosphere*, Ed. H.-J. Bolle, Science Press, Princeton, 630 pp.

Dave, J. V., 1971: Determination of size distribution of spherical polydispersions. *Appl. Opt.* **10**, 2035-2044.

Deirmendjian, D., 1969: *Electromagnetic Scattering on Spherical Polydispersion*. Elsevier, New York, 78 pp.

Gorchakov, G. I. and A. S. Yemilenko, 1974: Modeling the Atmospheric Aerosol Microstructure and the Light Scattering Matrix. *Izv.,, Atmos. Ocean. Phys.*, **10**, 211-216.

————, A. S. Yemilenko, Ye. A. Lykosov and V. G. Tolstobrov, 1976a: Determination of particle refractive index from the polarization of light scattered by foggy haze. *Izv., Atmos. Ocean. Phys.*, **12**, 83-86.

————, I. A. Gorchakova, Ye. A. Lykosov, V. G. Tolstobrov and L. S. Turovtseva, 1976b: Determination of the refractive index and microstructure of foggy haze. *Izv., Atmos. Ocean. Phys.*, **12**, 371-375.

Grams, G. W., I. H. Blifford, Jr., D. A. Gillette and P. B. Russell, 1974: Complex index of refraction of airborne soil particles. *J. Appl. Meteor.*, **13**, 459-471.

Grassl, H., 1971: Determination of aerosol size distributions from spectral attenuation measurements. *Appl. Opt.*, **10**, 2534-2538.

Hansen, M. Z., 1980: Atmospheric particle analysis using angular light scattering. *Appl. Opt.*, **19**, 3441-3448.

Heintzenberg, J., 1977: Particle size distributions from scattering data on nonspherical particles via Mie theory. in *Radiation in the atmosphere*, Ed. H.-J. Bolle, Science Press, Princeton, 630 pp.

———— and R. M. Welch, 1982: Retrieval of aerosol size distribution from angular scattering functions: effect of particle composition and shape. *Appl. Opt.*, **21**, 822-830.

Holland, A. C. and G. Gagne, 1970: The scattering of polarized light by polydisperse system of irregular particles. *Appl. Opt.*, **9**, 1113-1121.

van de Hulst, H. C., 1957: *Light scattering by small particles*. Wiley, New York, N.Y., 470 pp.

Junge, C. E., 1955: The size distribution and aging of natural aerosols as determined from electrical and optical data on the atmosphere. *J. Meteor.*, **12**, 13-25.

Liou, Kuo-Nan and J. E. Hansen, 1971: Intensity and polarization for single scattering by polydisperse spheres: A comparison of ray optics and Mie theory. *J. Atmos. Sci.*, **28**, 995-1004.

Patterson, E. M., 1977: Atmospheric extinction between 0.55 μm and 10.6 μm due to soil-derived aerosols. *Appl. Opt.*, **16**, 2414-2418.

Phillips, B. L., 1962: A technique for the numerical solution of certain integral equations of the first kind. *J. Assoc. Comp. Mach.*, **9**, 84-97.

Pinnick, R. G., D. E. Carroll and D. J. Hofmann, 1976: Polarized light scattered from monodisperse randomly oriented nonspherical aerosols: measurements. *Appl. Opt.*, **15**, 384-393.

Powell, R. S., R. R. Circle, D. C. Vogel, P. D. Woodson III and B. Donn, 1967: Optical scattering from nonspherical randomly aligned polydisperse particles. *Planet. Space. Sci.*, **15**, 1641-1652.

Reagan, J. A., D. M. Byrne, M. D. King, J. D. Spinhirne, and B. H. Herman, 1980: Determination of the complex refractive index and size distribution at atmospheric particulates from bistatic-monostatic lidar and solar radiometer measurements. *J. Geophys. Res.*, **85**, 1591-1599.

Shifrin, K. S., V. F. Turchin, L. S. Turovtseva and V. A. Gashko, 1972: Reconstruction of particle size distribution by statistical regularization of the scattered function. *Izv., Atmos. Ocean. Phys.*, **8**, 1268-1278.

———— and V. A. Gashko, 1974: Determination of the microstructure of a scattering medium consisting of a mixture of particles with differ-

ent indices of refraction. *Izv., Atmos. Ocean. Phys.*, **10**, 943-949.

Takamura, T. and M. Tanaka, 1978: Measurements of intensity and degree of polarization of light scattered by aerosols. *Sci. Rep. Tohoku Univ., Ser.* 5, **25**, 169-196.

Tanaka, M. and T. Nakajima, 1977: Effects of oceanic turbidity and index of refraction of hydrosols on the flux of solar radiation in the atmosphere ocean system. *J. Quant. Spectrosc. Radiat. Transfer*, **18**, 93-111.

Toon, O. B. and J. B. Pollack, 1976: A global averaged model of atmospheric aerosols for radiative transfer calculation. *J. Appl. Meteor.*, **15**, 225-246.

Turchin, V. F. and V. Z. Nozik, 1969: Statistical regularization of the solution of incorrectly posed problems. *Izv., Atmos. Ocean. Phys.*, **5**, 29-38.

Twitty, J. T., 1975: The inversion of aureole measurements to derive aerosol size distribution. *J. Atmos. Sci.*, **32**, 584-591.

Twomey, S., 1963: On the numerical solution of Fredholm integral equations of the first kind by the inversion of the linear system produced by quadrature. *J. Assoc. Comp. Mach.*, **10**, 97-101.

——— and H. B. Howell, 1967: Some aspects of the optical estimation of microstructure in fog and cloud. *Appl. Opt.*, **6**, 2125-2131.

Ward, G., K. M. Cushing, R. D. McPeters, and A. E. S. Green, 1973: Atmospheric aerosol index of refraction and size-altitude distribution from bistatic laser scattering and solar aureole measurements. *Appl. Opt.*, **12**, 2585-2592.

Weastwater, E. R. and A. Cohen, 1973: Application of Backus-Gilbert inversion technique to determination of aerosol size distribution from optical scattering measurements. *Appl. Opt.*, **12**, 1340-1348.

Yamamoto, G. and M. Tanaka, 1969: Determination of aerosol size distribution from spectral attenuation measurements. *Appl. Opt.*, **8**, 447-453.

Zaneveld, J. R. V., D. M. Roach and H. Pak, 1974: The determination of the index of refraction distribution of oceanic particulates. *J. Geophys. Res.*, **79**, 4091-4095.

光散乱測定による，大気中および海洋中の浮遊粒子の複素屈折率と粒径分布の同時決定

田中正之・中島映至・高村民雄*

東北大学理学部超高層物理学研究施設

光散乱測定によって，エアロゾルやハイドロゾルの複素屈折率と粒径分布を評価するために，インバージョン法とライブラリー法を同時に使うデータ解析法を提案する。詳細な数値実験の結果，この方法を散乱面に水平および垂直な散乱光の偏光成分の測定に適用すると，複素屈折率と粒径分布の真値を良く推定できることが明らかになった。

* 現在所属：防衛大学校